CACR-91-10

Angular Spectrum Modelling of Water Waves

Robert A. Dalrymple and James T. Kirby
Center for Applied Coastal Research
University of Delaware
Newark, DE 19716

To Appear in Reviews of Aquatic Sciences

Contents

1 Introduction

The propagation of water waves over an irregular bathymetry has served as an important area of research for mathematicians, oceanographers and ocean engineers for a long time due to the the importance of the problem and the mathematical difficulties encountered in its solution. For example, the design of shore facilities (harbors, breakwaters and piers) and offshore structures requires a good knowledge of the wave heights and directions to be encountered at the site of interest. This review will briefly discuss the history of wave modelling and then elaborate a new methodology for modelling of waves, the angular spectrum approach.

Numerous models have been proposed in the past to solve various aspects of wave propagation. The first models were ray tracing models, which determine the path followed by the waves as they traverse irregular bathymetry.[36,38] These models, when used either from offshore towards the shore or in reverse, provide reasonable estimates for wave heights when refraction (due to variations in water depth normal to the direction of propagation) and shoaling (due to changes in water depth in the wave direction) are the dominant phenomena affecting the waves.

Computer models of nearshore circulation have required knowledge of the wave field at discrete grid points over an offshore region, which led to the development of models based on the irrotationality of the wave number. Examples of these models are Perlin and Dean[42] and Dalrymple.[9] Despite the inclusion of numerous other effects (such as wave-current interaction and bottom friction by Dalrymple), none of these models incorporates the process of diffraction. Ebersole[17] extended these models to include diffraction.

Diffraction, which is the turning of the wave rays due to gradients in wave amplitude, as would occur as waves pass a surface-piercing obstacle (e.g., breakwaters), was largely ignored for coastal situations due to the lack of a suitable model which would incorporate refraction and diffraction simultaneously. In the vicinity of breakwaters, the optics solution of Sommerfeld[45] was adapted by Penney and Price[40] for waves; however, the procedure by which refraction models would be patched locally into the diffraction solution remained an art for many years.

Of fundamental importance to the combined refraction/diffraction problem was the development of the mild-slope equation by Berkhoff.[1] This equation, which is the vertically-averaged equation for wave motion, reduces the 3-D problem of solving the Laplace equation to a 2-D problem for cases where the bottom does not vary greatly. This second order partial differential equation permits refraction and shoaling, as well as diffraction, to occur simultaneously. Numerous finite element models were developed to solve this equation.[1,23,3]

Liu and Mei[30] first developed a parabolic approximation to the problem of wave fields in the vicinity of shore-parallel breakwaters, in order to study the wave-induced circulation caused by the presence of the structure.

Radder[43] developed the first parabolic representation of the mild-slope equation, leading to greater computational simplicity and the ability to neglect the downwave boundary condition, which in practice is very difficult to specify *a priori*. The parabolic modelling

has been explored more fully by Kirby and Dalrymple[28] and Liu and Tsay,[31] who showed how to develop a weakly-nonlinear version of the mild-slope equation, allowing for amplitude dispersion (bigger waves travel faster than smaller ones).

One of the drawbacks of the parabolic modelling has been the restriction that the waves travel almost in a prescribed direction. The small-angle parabolic models for example require that the waves travel within $\pm 30°$ of the x axis. Wider angle models have been developed by Booij[4] and Kirby;[25,26] however, each successive approximation only opens the range of allowed angles by a finite amount and the limit of full $\pm 90°$ is never approached. An alternative path taken by Lozano and Liu[33] was to base the parabolic model on the underlying refracted wave field, such that the large angles due to refraction were taken care of properly prior to the diffraction calculations. However, diffraction effects still only occurred in a narrow range of angles around the principle ray direction.

Angular spectrum modelling has in principle no limitation on wave angle; hence, its development for water waves by Dalrymple and Kirby,[12] Dalrymple, Suh, Kirby and Chae[15] and Suh, Dalrymple and Kirby.[49] The angular spectrum approach has been used in other fields, such as radio astronomy (Booker and Clemmow[5]) and electromagnetic fields (Clemmow[8]). Some references for the development of angular spectra are Goodman[20] (optics) and Stamnes[47] (optics and water waves).

The basic ideas behind the angular spectrum can be obtained by examining a single wave train on the surface of the ocean, which can be described at a point (x, y) in the horizontal plane as

$$\eta(x, y, t) = a\, e^{i(k\cos\theta\, x + k\sin\theta\, y - \omega t)} \tag{1}$$

where the real part of η is the displacement of the water surface about its mean position, a is the wave amplitude, k and ω are the wave number (defined as 2π over the wave length L) and the angular frequency (2π over the wave period T), respectively. The angle θ is the direction that the wave direction makes with the x axis, which points onshore. At x=0, the wave form can be separated into two parts,

$$\eta(0, y, t) = a e^{ik\sin\theta\, y} e^{-i\omega t} \tag{2}$$

Clearly there is a oscillatory variation of η in the y direction, which will be denoted by $\tilde{\eta}(y)$. Defining λ as $k\sin\theta$ we have

$$\tilde{\eta}(y) = a e^{i\lambda y} \tag{3}$$

For a more realistic sea state, the functional form of $\tilde{\eta}(y)$ will be more complicated, say, $f(y)$, resulting from the superimposition of many wave trains with different directions, but with the same frequency ω. To determine the contributions of each of the many wave trains in $f(y)$, we can decompose it through the use of a Fourier transform in the y direction. The Fourier transform and its inverse for any function $f(y)$ defined on an infinitely wide domain are given by

$$\begin{aligned} \hat{f}(\lambda) &= \int_{-\infty}^{\infty} f(y) e^{-i\lambda y} dy \\ f(y) &= \frac{1}{2\pi} \int_{-\infty}^{\infty} \hat{f}(\lambda) e^{i\lambda y} d\lambda \end{aligned} \tag{4}$$

where the Fourier transform parameter is λ. The angular spectrum is $\hat{\eta}(\lambda)$, which consists of the amplitudes of the wave trains travelling in directions, $\theta = \sin^{-1}(\lambda/k)$. Thus, the angular spectrum is a (continuous) collection of wave trains, each travelling in a different direction, determined by the Fourier parameter, λ. The free surface displacement is now expressed as

$$\eta(x,y,t) = \frac{1}{2\pi}\int_{-\infty}^{\infty} \hat{\eta}(\lambda) e^{i\sqrt{k^2-\lambda^2}\,x} e^{i\lambda\,y} d\lambda \tag{5}$$

where $k\cos\theta$ is rewritten as $\sqrt{k^2-\lambda^2}$ using the definition of λ. (We note that the contributions from the integral from $|\lambda| > k$ are not propagating waves, as they decay in the x direction.)

2 The Angular Spectrum Model

The sea surface for many years has been described by a superposition of individual wave trains travelling in different directions, leading to a directional spectrum. The angular spectrum is very similar except that the directions are prescribed by Fourier analysis for each frequency, as we now show.

The directional frequency spectrum, $|F(\omega,\theta)|^2$, may be defined via the definition of the water surface,

$$\eta(x,y,t) = \int_0^{\infty}\int_{-\pi}^{\pi} F(\omega,\theta)\, e^{i(k\cos\theta x + k\sin\theta y - \omega t)} d\theta d\omega \tag{6}$$

where the real part of η is the water surface elevation as a function of time at position (x,y). $F(\omega,\theta)$ is the amplitude spectrum for the waves. If we now assume that we can separate $F(\omega,\theta)$ into a separate frequency and direction components, $F = S(\omega)D(\theta)$ then the above expression can be rewritten (replacing $k\sin\theta$ with the parameter λ and $k\cos\theta$ with $\sqrt{k^2-\lambda^2}$) as

$$\eta(x,y,t) = \int_0^{\infty} S(\omega)\left\{\int_{-k}^{k} \frac{D(\theta)}{\sqrt{k^2-\lambda^2}}\, e^{\pm i\sqrt{k^2-\lambda^2}x} e^{i\lambda y} d\lambda\right\} e^{-i\omega t} d\omega \tag{7}$$

For the present time we will restrict ourselves to a single frequency, ω_0, with an amplitude, $S_0 = S(\omega_0)d\omega$, and define the water surface of the waves at the frequency ω_0 as

$$\eta_{\omega_0}(x,y,t) = \int_{-k}^{k} S_0 \frac{D_1(\lambda)}{\sqrt{k^2-\lambda^2}} e^{\pm i\sqrt{k^2-\lambda^2}x} e^{i\lambda y} d\lambda \tag{8}$$

where the direction spreading function $D(\theta)$ has been transformed into $D_1(\lambda) = D(\sin^{-1}(\lambda/k))$. The angular spectrum is defined as the complex amplitude of the waves,

$$A(\lambda) \equiv \frac{2\pi S_0 D_1(\lambda)}{\sqrt{k^2-\lambda^2}}$$

The wave trains making up the angular spectrum are progressive (that is, $\sqrt{k^2-\lambda^2}$ is real); however, for convenience and for analogy to the Fourier transform, we change the limits of

integration to $\pm\infty$.

$$\eta_{\omega_0}(x,y,t) = \frac{1}{2\pi}\int_{-\infty}^{\infty} A(\lambda) e^{\pm i\sqrt{k^2-\lambda^2}\,x} e^{i\lambda y} d\lambda \tag{9}$$

The new additional wave trains that are added by extending the range of integration are all evanescent, decaying, for example, in the $+x$ direction as λ is greater than k and the x dependency becomes $\exp\{-\sqrt{\lambda^2-k^2}\;x\}$. In this form, the wave spectrum now looks like the Fourier transform (5).

Henceforth, we will restrict the waves to propagation in the $+x$ direction, keeping only the positive sign in the exponent.

For a domain which repeats periodically in the transverse direction (y), we have the following Fourier transform pair,

$$\hat{f}_n(x,t) = \frac{1}{2b}\int_{-b}^{b} f(x,y,t) e^{-in\lambda y} dy \tag{10}$$

$$f(x,y,t) = \sum_{-\infty}^{\infty} \hat{f}_n e^{in\lambda y} \tag{11}$$

where $\hat{f}_n$ is the wave contribution associated with the Fourier parameter value of $n\lambda$, now $\lambda = \pi/b$ and $2b$ is the width of the domain. The equivalent angular spectrum to Eq. 9 for a given frequency is

$$\eta(x,y,t) = \sum_{-\infty}^{\infty} A_n e^{i\sqrt{k^2-(n\lambda)^2}\,x} e^{in\lambda y} \tag{12}$$

which is an infinite sum of discrete wave trains, each of amplitude, A_n, propagating in discrete directions, measured by the angle θ_n to the x axis,

$$\theta_n = \tan^{-1}\left(\frac{n\lambda}{\sqrt{k^2-(n\lambda)^2}}\right) \text{ for } n\lambda < k \text{ and } n = 1,2,3,\ldots \tag{13}$$

Again, evanescent modes occur when $n\lambda > k$. Figure 1 shows a schematic of the angular spectrum, showing a number of wave directions. Sometimes these individual wave trains will be referred to as Fourier modes or simply modes.

For domains bounded laterally by impermeable barriers, solutions are sought in the form

$$f(x,y,t) = \sum_{n=0}^{\infty} \hat{f}\cos n\lambda y \tag{14}$$

where again $\lambda = \pi/b$, in order that

$$\frac{\partial f}{\partial y} = 0, \quad \text{at } y = \pm b,$$

or, for solutions which are non-symmetric about $y = 0$,

$$f(x,y,t) = \sum_{n=0}^{\infty} \hat{f}_e \cos n\lambda y + \sum_{n=0}^{\infty} \hat{f}_o \sin \gamma_n y \tag{15}$$

where the first series represents the even solution (symmetric about $y = 0$) and the second series is the antisymmetric part of the solution. The parameter $\gamma_n = (n+\frac{1}{2})\pi/b$.

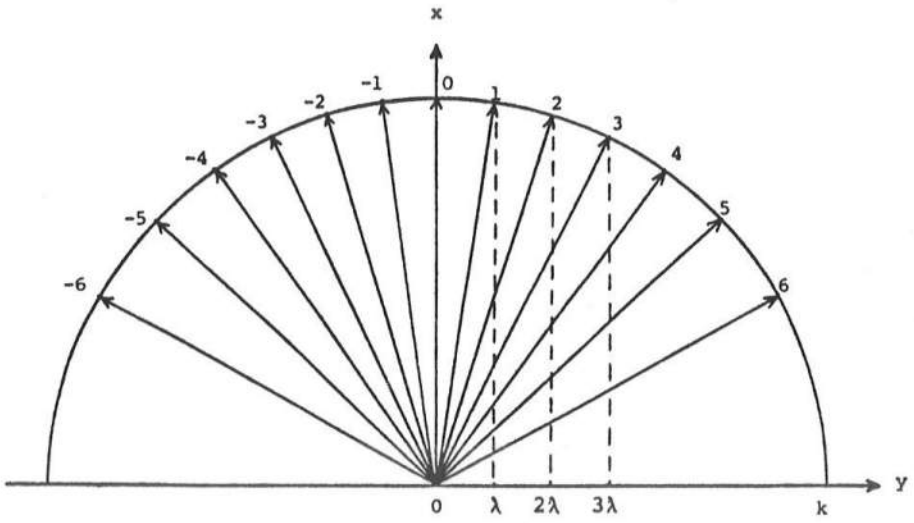

Figure 1: The Angular Spectrum

3 Constant Depth Solutions

To fix ideas and to illustrate the use of Fourier transforms in solving the wave problem, consider the following coordinate system: the onshore direction is the x direction and the transverse direction is the y direction; the coordinate z will point upward from the mean water level. The velocity potential for the wave motion is $\Phi(x, y, z, t)$, from which the velocities and water surface elevation can be determined (see, e.g., Dean and Dalrymple;[16] Chap. 4). For linear plane waves on constant depth, the boundary value problem is separable and the reduced potential $\phi(x, y)$ must satisfy the Helmholz equation,

$$\frac{\partial^2 \phi}{\partial x^2} + \frac{\partial^2 \phi}{\partial y^2} + k^2 \phi = 0 \tag{16}$$

where the total velocity potential is

$$\Phi(x, y, z, t) = \phi(x, y) \frac{\cosh k(h + z)}{\cosh kh} \, e^{-i\omega t},$$

and the wave number k and the angular wave frequency ω are related through the dispersion relationship, which results from the linear free surface boundary conditions,

$$\omega^2 = gk \tanh kh \tag{17}$$

Fourier transforming the differential equation in the y direction yields an equation for the transformed reduced potential

$$\frac{d^2 \hat{\phi}}{dx^2} + (k^2 - \lambda^2) \, \hat{\phi} = 0, \tag{18}$$

which is an ordinary differential equation for $\hat{\phi}(x)$. The solution for waves propagating in the $+x$ direction is

$$\hat{\phi}(x) = Ae^{i\sqrt{k^2-\lambda^2}x} \tag{19}$$

where A is a function of λ (but constant in x) which must be determined. The Fourier inverse in an infinitely wide domain is

$$\phi(x,y) = \frac{1}{2\pi}\int_{-\infty}^{\infty} A(\lambda)\, e^{i(\sqrt{k^2-\lambda^2}x+\lambda y)}\, d\lambda \tag{20}$$

At $x = 0$,

$$\phi(0,y) = \int_{-\infty}^{\infty} A(\lambda)e^{i\lambda y}d\lambda \tag{21}$$

Comparing with Equations (4), we see the boundary condition for $A(\lambda)$,

$$A(\lambda) = \int_{-\infty}^{\infty} \phi(0,y)e^{-i\lambda\, y}dy \tag{22}$$

It should be emphasized that the solution we have obtained (20, 22) for this linear wave field is *fixed by the boundary condition at* $x = 0$, as there is no coupling between the various modes comprising the angular spectrum. If the problem of interest is wave propagation behind a breakwater, with all the attendent diffraction, the angular spectrum model shows that the wave behavior is *solely* determined by the boundary condition, *i.e.*, the diffraction the waves experience behind a breakwater is determined by the boundary condition at the breakwater as each of the wave trains comprising the angular spectrum propagate independently of each other. The diffraction pattern observed is created by the radial spreading of the wave trains comprising the angular spectrum.

Mathematically, the classical Fourier transform is defined for functions which are absolutely integrable,

$$\int_{\infty}^{\infty} |\phi(0,y)|\, dy < 0$$

However, for periodic initial conditions, such as an oblique wave train, say $\phi(0,y) = a\, e^{ik\sin\theta y}$, this condition is not satisfied. We use instead *generalized* Fourier transforms, e.g., Papoulis[39] (Chapter 3), who shows, for example, that the Fourier transform of $e^{i\lambda_0 y}$ is $2\pi\delta(\lambda-\lambda_0)$, where δ is a Dirac delta function.

For a periodic domain of lateral extent $2b$, the Fourier transform leads to

$$\frac{d^2\hat{\phi}_n}{dx^2} + (k^2 - (n\lambda)^2)\hat{\phi}_n = 0 \tag{23}$$

with the solution

$$\hat{\phi}_n(x) = A_n e^{i\sqrt{k^2-(n\lambda)^2}\, x} \tag{24}$$

The inverse is

$$\Phi(x,y,z,t) = \sum_{-\infty}^{\infty} A_n\, e^{i(\sqrt{k^2-(n\lambda)^2}\, x+n\lambda\, y-\omega t)}\, \frac{\cosh k(h+z)}{\cosh kh} \tag{25}$$

The wave number vector $\vec{k} = (k\cos\theta, k\sin\theta) = (\sqrt{k^2 - (n\lambda)^2}, n\lambda)$.

Again, the behavior of the wave trains as they propagate is fixed by the boundary condition in this problem, which is given by a Fourier transform of the boundary conditions, $\hat{\phi}_n(0) = A_n$. For example, for a plane wave train propagating at angle, γ to the x axis, the boundary value of $\phi(0,y) = Be^{i\lambda_0 y}$, where $\lambda_0 = k\sin\gamma$. The Fourier transform of this boundary condition, again for a periodic domain, is

$$A_n = B\frac{\sin(\lambda_0 - n\lambda)b}{(\lambda_0 - n\lambda)b},$$

unless $\lambda_0 = m\lambda$ for some integer, m, in which case all the A_n are zero, except for A_m, which is B. For computational purposes, it is convenient to chose incident plane wave trains which correspond to this condition.

The conservation of energy equation can be used as a check for numerical calculations in periodic domains, as the energy fluxes through the lateral boundaries cancel and therefore the flux of energy across any plane parallel to the y axis is a constant. If the energy flux is defined as

$$\mathcal{F} = -\int_{-b}^{b} \rho\frac{\partial\Phi}{\partial t}\frac{\partial\Phi}{\partial x}dydz, \tag{26}$$

then the flux past any location in terms of the Fourier coefficients, A_n, can be shown to be

$$\rho\omega\frac{CC_g}{g}b\sum_{n}^{n_p}|A_n|^2\sqrt{k^2 - (n\lambda)^2} = \text{ constant} \tag{27}$$

3.1 Wavemakers

The solution for $\phi(x,y)$ in constant depth water (20,22) can be used to determine the wave field inside directional wave basins, which are typically rectangular basins with segmented wavemakers along one wall.[11] For an example, we will assume the basin is infinitely wide (y direction) with the x axis located at the center of the wavemaker pointing into the basin.

Equation (21) indicates that the wave field is known once the velocity potential is specified along the wavemaker; however, the usual linearized wavemaker boundary condition specifies the velocity in the x direction at x=0 (see Dean and Dalrymple,[16] for example). Therefore we need to treat this problem slightly differently.

We will take the horizontal velocity created by the wavemaker of length $2a$ (associated with the progressive wave mode) to be adequately described by

$$\frac{d\phi(0,y)}{dx} = \begin{cases} Ue^{i\lambda_0 y}, & |y| < a \\ 0, & |y| > a \end{cases} \tag{28}$$

where $\lambda_0 = k\sin\gamma$ and γ measures the desired wave direction. The Fourier transform of this condition is

$$\frac{d\hat{\phi}(0,\lambda)}{dx} = \frac{2U\sin(\lambda_0 - \lambda)a}{(\lambda_0 - \lambda)} \tag{29}$$

From the solution for $\phi(x, y)$, we have

$$\frac{d\phi(0,y)}{dx} = \frac{1}{2\pi}\int_{-\infty}^{\infty} i\sqrt{k^2-\lambda^2}\, A(\lambda)\, e^{i\lambda y}\, d\lambda \tag{30}$$

and, after transforming,

$$\frac{d\hat{\phi}(0,\lambda)}{dx} = i\sqrt{k^2-\lambda^2}A(\lambda) \tag{31}$$

Equating these two expressions for the transformed velocity, we find

$$A(\lambda) = -\frac{2iU\sin(\lambda_0-\lambda)a}{(\lambda_0-\lambda)\sqrt{k^2-\lambda^2}} \tag{32}$$

This gives the final form for the velocity potential in the basin

$$\phi(x,y) = -\frac{i}{2\pi}\int_{-\infty}^{\infty} \frac{2U\sin(\lambda_0-\lambda)a}{(\lambda_0-\lambda)}\, \frac{e^{i\sqrt{k^2-\lambda^2}\,x}}{\sqrt{k^2-\lambda^2}}\, e^{i\lambda y}\, d\lambda \tag{33}$$

The convolution theorem allows this expression to be rewritten into the form shown by Dalrymple and Greenberg[11] and Dalrymple and Kirby,[12]

$$\phi(x,y) = \frac{iU}{2}\int_{-a}^{a} e^{i\lambda\zeta}\, \mathrm{H}_0^{(1)}(k\sqrt{x^2-(y-\zeta)^2})\, d\zeta \tag{34}$$

which is also obtainable through a Greens function approach. Dalrymple and Greenberg[11] also treated the evanescent modes which are important in the vicinity of the wavemaker. Stamnes[47] shows how to obtain the evanescent modes in the context of an angular spectrum.

Dalrymple and Kirby[12] point out that the wave field behind a thin island of width $2a$ can be easily found by taking the plane wave solution and subtracting the wavemaker solution from it, according to Babinet's Principle (from optics, e.g. Born and Wolf,[6] §11.3).

Dalrymple[10] has used this constant depth solution and the non-symmetric Fourier expansion (15) to determine the wave fields generated by directional wavemakers in basins of finite width, taking into account side wall reflection. This is the so-called 'designer waves' solution. (His solution is also valid for basins with straight and parallel bottom contours.)

To illustrate the 'designer wave' concept, see Figure 2, which show the instantaneous water surface for a wave train with 30° angle of incidence which is generated at the wavemaker, located at the bottom of the figure. Due to the presence of the reflecting wall at the left of the figure, a short-crested wave pattern is created. The presence of the side wall at the right of the figure creates a diffraction zone. There is only a limited portion of the wave basin near the wavemakers, where the desired wave train exists. At the far end of the tank (at the top of the figure), the wave field is clearly no longer a uniform wave train. Now, if a long-crested wave train is desired to occur at the far end of the tank, then the power of a directional wavemaker can be used. By generating a nonuniform wave field, the presence of the side walls can be incorporated in the wavemaker signals. For example, to generate a wave train with 30° angle of incidence at the far end of the basin, the wavemaker must generated

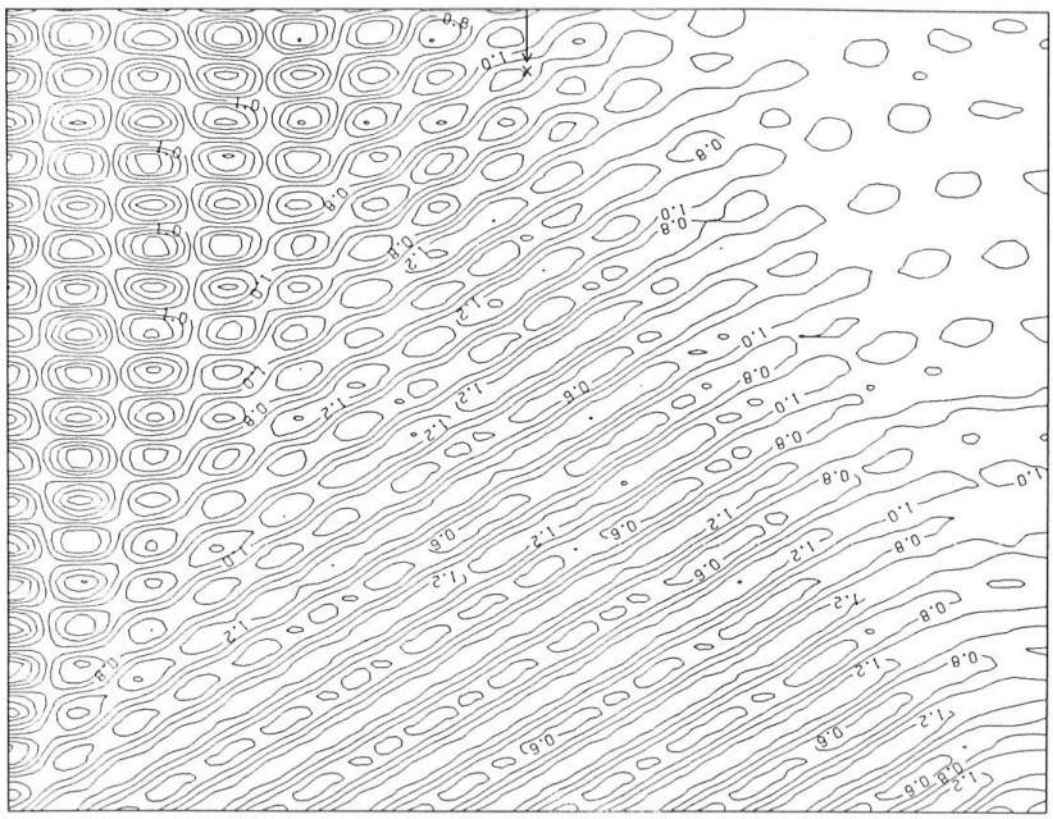

Figure 2: Instantaneous Wave Field Generated by a Directional Wavemaker in a Basin with Reflecting Sidewalls, from Dalrymple (1989)

short-crested and diffracted waves. For this case, if we now imagine the wavemaker at the top of the same figure, we see that by the time the wave field propagates to the far end of the tank (now the bottom of Figure 2), the wave becomes long-crested. This technique, including shoaling waves, is used in the Ocean Engineering Laboratory at the University of Delaware.

3.2 Waves Behind Narrow Gaps

Another interesting application of this constant depth solution is the propagation of a directional sea through a small gap, which could be, for example, a natural gap fronting an embayment, or a man-made gap, as between two breakwater segments. It has been noticed that, regardless of how directional the sea state is seaward of the gap, the waves inshore of the gap are long-crested and circular in plan.

This problem can be treated in several ways. First, the influence of the waves on the seaward side of the breakwater could be neglected, in which case the wavemaker solution, developed above, could be used directly with the appropriate specification of the velocity in the gap. More correctly, the offshore wave field can be specified and matched at the gap to the wave field on the sheltered side of the breakwater. This is the method we will use.

We postulate an angular spectrum for the waves offshore of the (infinitessimally narrow) gap for a given frequency as

$$\phi_o(x,y) = \frac{1}{2\pi}\int_{-\infty}^{\infty} A(\lambda)\, e^{i\sqrt{k^2-\lambda^2}x}\, e^{i\lambda y} d\lambda \tag{35}$$

where the $A(\lambda)$ are imposed by the nature of the offshore sea state. The velocity at the gap is

$$\frac{\partial \phi_o(0,y)}{\partial x} = \frac{1}{2\pi}\int_{-\infty}^{\infty} i\sqrt{k^2-\lambda^2}\, A(\lambda) e^{i\lambda y}\, d\lambda\, \delta(y) \tag{36}$$

where the $\delta(y)$ is the Dirac delta function, which represents the fact that the velocity is zero except at the narrow gap. The Fourier transform:

$$\frac{\partial \hat{\phi}_o(0,y)}{\partial x} = \frac{1}{2\pi}\int_{-\infty}^{\infty} i\sqrt{k^2-\lambda^2}\, A(\lambda)\, d\lambda \tag{37}$$

Inside the (infinitely thin) breakwater, the wave field for this frequency is given by another angular spectrum,

$$\phi_i(x,y) = \int_{-\infty}^{\infty} B(\lambda)\, e^{i\sqrt{k^2-\lambda^2}x}\, e^{i\lambda y}\, d\lambda \tag{38}$$

The transformed horizontal velocity (x direction) at the gap is

$$\frac{\partial \hat{\phi}_i(0,y)}{\partial x} = i\sqrt{k^2-\lambda^2}\, B(\lambda) \tag{39}$$

Equating both of the velocities yields

$$B(\lambda) = \frac{1}{2\pi}\frac{\int_{-\infty}^{\infty}\sqrt{k^2-\lambda^2}\, A(\lambda)\, d\lambda}{\sqrt{k^2-\lambda^2}} \tag{40}$$

We can make several assumptions here for $A(\lambda)$. If we assume that the wave trains are coming from all directions with the same height (a), then $A(\lambda) = a$; alternatively if the waves come only from the direction associated with λ_0, then $A(\lambda) = A(\lambda_0)\delta(\lambda_0 - \lambda)$. For both cases, the integral in the above expression can be evaluated, such that

$$B(\lambda) = \frac{ak^2}{4\sqrt{k^2-\lambda^2}} \tag{41}$$

or

$$B(\lambda) = \frac{-iA(\lambda_0)}{\sqrt{k^2-\lambda^2}} \tag{42}$$

Substituting these expression into the angular spectrum inside the breakwater, (38), and integrating, we have

$$\phi_i(x,y) = \alpha \mathrm{H}_0(kr) \tag{43}$$

where, for the first case, $\alpha = ak^2/2$ and, for the second case, $\alpha = -iA(\lambda_0)/2$. The Hankel function of the first kind and order zero, which is a function of the wavenumber and the radial distance $r = \sqrt{x^2+y^2}$, arrives through the following identity:

$$\frac{1}{2\pi}\int_{-\infty}^{\infty} \frac{e^{i\sqrt{k^2-\lambda^2}x}\, e^{i\lambda y}\, d\lambda}{\sqrt{k^2-\lambda^2}} = \frac{1}{2}\,\mathrm{H}_0(kr) \tag{44}$$

The nature of our solution for one frequency is that the wave form inside the bay, which is only dependent on the radial distance from the gap, is described by circular wave crests (via the Hankel function). For the linear superposition of many frequencies, the same result obtains–all frequencies are described by circular wave crests. (For waves through a breakwater gap much smaller than a wavelength, the result is not new, Penney and Price.[40])

Dalrymple and Martin[13] examine the wave field inshore of a line of breakwaters that are separated by gaps of the same length (similar to an optical grating). The influence of the offshore waves is included in their analysis. They find that the wave field inshore of the breakwater can be very complicated as new wave modes are generated when the gap spacing is less than a wave length, due to superposition of the diffraction patterns behind each gap. The presence of multiple wave trains of the same frequency can lead to the formation of rip currents behind such structures.

3.3 Wave Focussing

Stamnes *et al.*[48] carried out a laboratory and theoretical study of the focussing of waves behind a shoal, designed to act as a Fresnel lens. The field experiment consisted of generating a circular wave with a point wavemaker; these waves were focussed by the lens to another (focal) point. Wave height measurements were made with densely spaced transects in the vicinity of the focal point. The comparisons to the data were made using the linear constant depth angular spectrum approach, along with a nonlinear parabolic model. The comparison was carried out by assuming the boundary condition for the wave field over the lens was representable by a arc of a circular wave converging on the focal point. The comparisons for their tests show that the basic features of the experiment are describable by the angular spectrum, but that wave nonlinearity in the vicinity of the focal point is crucial for agreement.

4 Variable Bathymetry

Most coastal regions of interest are not characterized by uniform depth, but instead have spatial nonuniformity in bathymetry. Generally, this spatial variation is characterized by a trend of decreasing depth in the shoreward direction, with a superposed, irregular depth

variation in both the on-offshore and longshore direction. For the case of intermediate water depth, it is convenient to model small amplitude waves using the mild-slope equation,[1,46]

$$\nabla \cdot CC_g \nabla\phi + k^2 CC_g \phi = 0 \tag{45}$$

which is applied separately to each frequency component in the wave train. Here, $\nabla(= \frac{\partial}{\partial x}\vec{i} + \frac{\partial}{\partial y}\vec{j})$ is the horizontal gradient operator, C is the wave phase celerity, and C_g is the group velocity of the waves, given by

$$C(x,y) = \omega/k(x,y) \tag{46}$$

$$C_g(x,y) = \frac{1}{2}\left(1 + \frac{2kh}{\sinh 2kh}\right) C \tag{47}$$

Again, the complete velocity potential is $\Phi(x,y,z,t) = \phi(x,y)e^{-i\omega t}\cosh k(h+z)/\cosh kh$. The coefficients, C and C_g, in (45) are determined based on the local value of the water depth $h(x,y)$ at each point in the domain of interest and the dispersion relationship (17).

4.1 Straight and Parallel Contours

The Fourier transform of (45) for an infinitely wide domain where the depth only varies in the x direction is

$$\frac{d}{dx}\left(CC_g \frac{d\hat{\phi}}{dx}\right) + (k^2 - \lambda^2)CC_g\hat{\phi} = 0 \tag{48}$$

This ordinary differential equation for $\hat{\phi}$ has variable coefficients as the wave number, wave phase, and group velocities vary with the depth, $h(x)$.

An assumed form of the solution for $\hat{\phi}$ is

$$\hat{\phi}(x) = \tilde{\phi}(x)e^{i\int\sqrt{k^2-\lambda^2}dx} \tag{49}$$

where $\tilde{\phi}$ is assumed to vary slowly in x as the exponential term carries most of the phase information and the integral is necessary to get the phase change with x correctly. Substituting into equation (48) leaves an equation for $\tilde{\phi}$,

$$2CC_g\sqrt{k^2-\lambda^2}\frac{d\tilde{\phi}}{dx} + \frac{d\left(CC_g\sqrt{k^2-\lambda^2}\right)}{dx}\tilde{\phi} = 0 \tag{50}$$

where we have neglected two small terms,

$$CC_g\frac{d^2\tilde{\phi}}{dx^2} \text{ and } \frac{\partial CC_g}{\partial x}\frac{d\tilde{\phi}}{dx}, \tag{51}$$

which are small compared to the remaining terms, as the bottom varies slowly in x as does $\tilde{\phi}$.

The resulting equation is a first order differential equation for the wave modes which can be solved by separation, resulting in

$$\tilde{\phi} = A_0 \frac{\sqrt{CC_g\sqrt{k^2-\lambda^2}}_0}{\sqrt{CC_g\sqrt{k^2-\lambda^2}}} = A_0 K_s(\lambda) K_r(\lambda) \tag{52}$$

or

$$\hat{\phi} = A_0 K_s K_r e^{i\int\sqrt{k^2-\lambda^2}dx} \tag{53}$$

where the terms with a zero subscript are evaluated at the origin. This equation shows that the (transformed) wave form is given by an initial amplitude, A, evaluated at $x = 0$ and then the wave changes with x in accordance with standard shoaling and refraction coefficients, $K_s K_r$. Furthermore there is no interaction between the different Fourier modes; any diffraction observed for $x > 0$ is due to the spreading of the angular spectrum, as each wave train propagates in a different direction.

The inverse Fourier transform yields

$$\phi = \frac{1}{2\pi}\int_{\infty}^{\infty} AK_s K_r e^{i\int\sqrt{k(x)^2-\lambda^2}dx} e^{i\lambda y} d\lambda \tag{54}$$

for an infinitely wide domain. This is a generalization of the result of Mei *et al.*,[34] who used a multiple scales approach, to now include all possible wave trains in a directional sea.

Dalrymple and Kirby[12] studied the case of waves propagating through gaps in a row of periodically spaced offshore breakwaters, assuming that the potential through the gaps could be given as the wave potential in the absence of the breakwaters (known as the Kirchoff approximation in optics). Shoreward of the breakwater the assumed planar bottom sloped upwards to the shoreline. Their results, see Figure 3, show diffraction patterns behind each of the breakwater gaps as would be expected, including the refraction of the waves due to the sloping bottom. There is also a region of short-crested waves due to the influence of neighboring gaps.

4.2 Realistic Bathymetry

For more realistic bathymetry, we must permit a variation in the bathymetry in the y direction as well. It is convenient to modify the mild-slope equation to treat this problem. Introducing $p(x,y) = CC_g$ and $\tilde{\phi} = \sqrt{p}\phi$, we obtain a Helmholz equation for the modified potential,

$$\nabla^2\tilde{\phi} + k_c^2\tilde{\phi} = 0 \tag{55}$$

where

$$k_c^2 = k^2 - \frac{\nabla^2\sqrt{p}}{\sqrt{p}} \tag{56}$$

Following Dalrymple *et al.*, 1989, a laterally averaged wave number is introduced for a domain of width,$2b$,

$$\overline{k^2} = \frac{1}{2b}\int_0^b k_c^2 dy$$

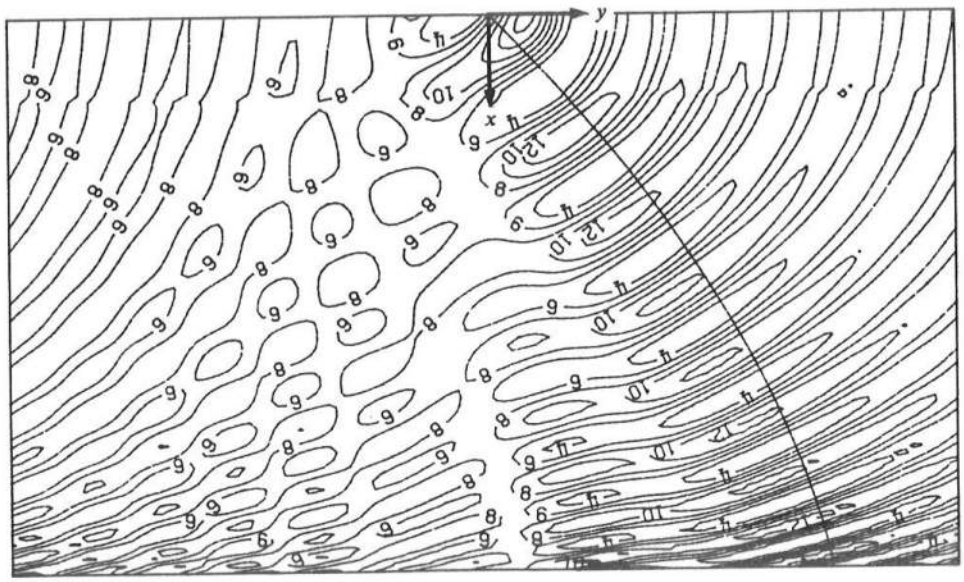

Figure 3: Instantaneous Wave Field Behind a Breakwater Gap Over a Sloping Bottom, from Dalrymple and Kirby (1988)

This permits rewriting the Helmholtz equation as

$$\nabla^2\tilde{\phi} + \overline{k^2}\phi - \overline{k^2}\nu^2\phi = 0 \tag{57}$$

where $\nu^2(x,y)$ represents the lateral deviation of $\bar{k}(x)$ from $k_c(x,y)$:

$$\overline{k^2}\nu^2 = \overline{k^2} - k_c^2.$$

For bathymetries which have very little variation in the y direction, the ν^2 term is small.

Fourier transforming (57) yields an equation for the Fourier modes,

$$\frac{d^2\hat{\phi}}{dx^2} + (\overline{k^2} - \lambda^2)\hat{\phi} - \overline{k^2}F(\nu^2\tilde{\phi}) = 0 \tag{58}$$

where the Fourier transform of the product, $\nu^2\tilde{\phi}$ is shown symbolically with the F operator.

This second order differential equation can be separated into two equations (as is done for developing parabolic equations), one equation governing waves propagating in the positive x direction and another for the opposite direction, which, after assuming that the negatively propagating wave motion is small, due to only small amounts of reflection, yields one equation,

$$\frac{d\hat{\phi}(x,\lambda)}{dx} = i\sqrt{\overline{k^2} - \lambda^2}\hat{\phi} - \frac{\left(\sqrt{\overline{k^2} - \lambda^2}\right)_x}{2\sqrt{\overline{k^2} - \lambda^2}}\hat{\phi} - \frac{i\,\overline{k^2}F(\nu^2\tilde{\phi})}{2\sqrt{\overline{k^2} - \lambda^2}} \tag{59}$$

The second term on the right hand side, which involves the x derivative of the square root term, is the shoaling and refraction term, which occurs for planar bathymetry, and the last term represents the effect of the irregular bathymetry. This bathymetric effect represents a coupling between all Fourier wave modes and the bottom due to refraction. Modes which do not exist in the initial conditions can be created by this interaction. For a periodic domain, as used in practice, the equivalent equation to (59) for each wave mode is

$$\frac{d\hat{\phi}_n(x,\lambda)}{dx} = i\sqrt{\overline{k^2} - (n\lambda)^2}\hat{\phi}_n - \frac{\left(\sqrt{\overline{k^2} - (n\lambda)^2}\right)_x}{2\sqrt{\overline{k^2} - (n\lambda)^2}}\hat{\phi}_n - \frac{i\,\overline{k^2}F_n(\nu^2\tilde{\phi})}{2\sqrt{\overline{k^2} - (n\lambda)^2}} \tag{60}$$

$$n = 0, \pm 1, \pm 2, \ldots, \pm\left(\frac{N}{2} - 1\right), -\frac{N}{2} \tag{61}$$

This equation represents N coupled ordinary differential equations, which may be solved by Runge-Kutta methods. However, not all of the Fourier modes need be calculated, since many of them are evanescent.

The example used by Dalrymple, Suh, Kirby and Chae[15] is that of a circular shoal located in a region of constant depth, as studied in the laboratory by Ito and Tanimoto.[24] The evolution of the modes over and behind the shoal are shown in Figure 4. The incident wave train is specified to have only one direction (mode). As the wave train encounters the shoal, the waves refract and focus due to the depth changes. Through the bottom term, new

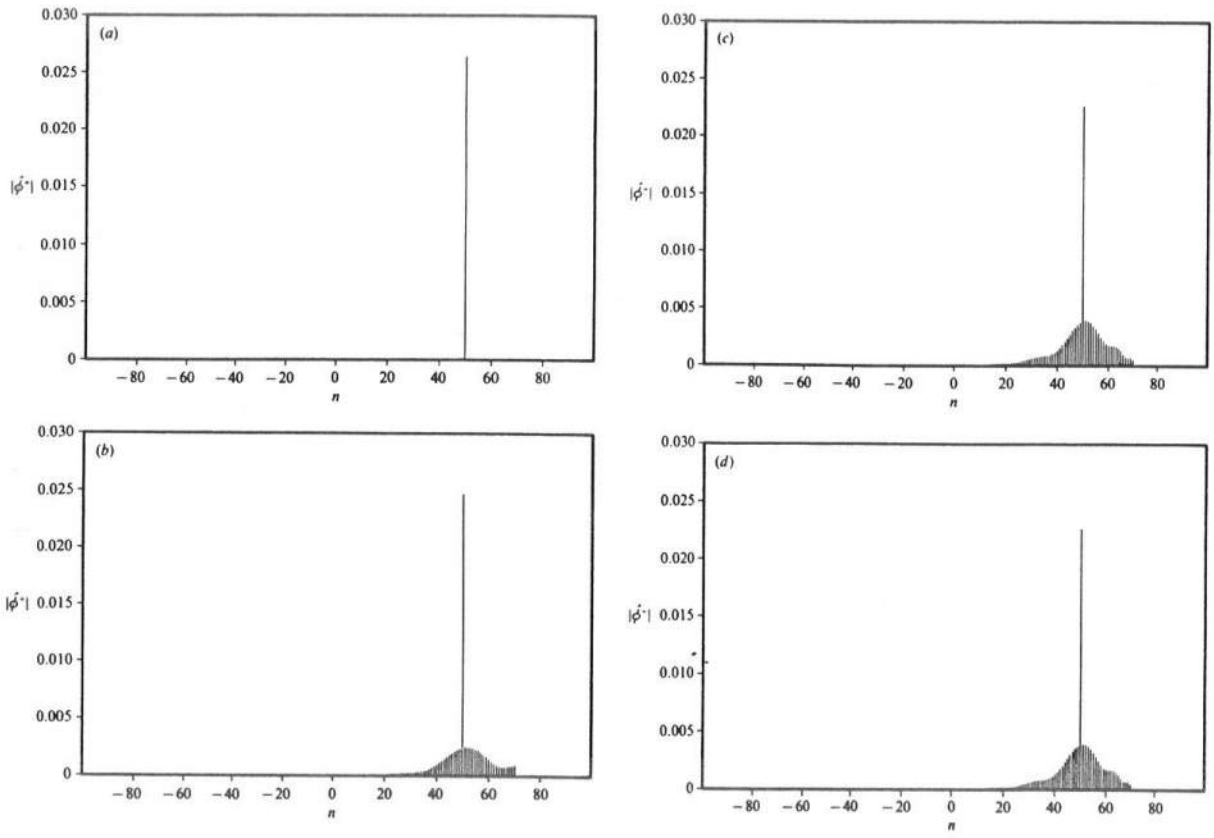

Figure 4: Evolution of the Angular Spectrum over a Circular Shoal, from Dalrymple *et al.*, 1989. (a) Seaward of Shoal, (b) Over the Top of the Shoal, (c) Just Landward of the Shoal, (d) Far Landward of the Shoal (note: no change from (c) to (d)).

Fourier modes are spawned and grow over the shoal. Behind the shoal, in the constant depth region, the bottom coupling term is no longer active and the angular spectrum is unchanged with further propagation distance, yet the wave field experiences the formation of a strong focal region, where diffraction is important. The apparent diffraction once again is explained by the radial propagation of the individual members of the angular spectrum, generated by refraction over the shoal. The envelope of the wave field in the vicinity of the shoal is shown in Figure 5

4.3 Alternative Formulation of the Bottom Coupling Term

Due to the efficiency of the FFT algorithm, the Fourier transform of the last term in (59) and the inverse transform needed to obtain $\tilde{\phi}$ from $\hat{\phi}$ are usually evaluated over a periodic interval in a finite width domain. Using this fact about the computational procedure allows the effect of the coupling term to be directly interpreted in terms of mode coupling between transverse surface wave modes and transverse bottom modes. In order to show this, let

$$f(y) = \nu^2 \tilde{\phi} \tag{62}$$

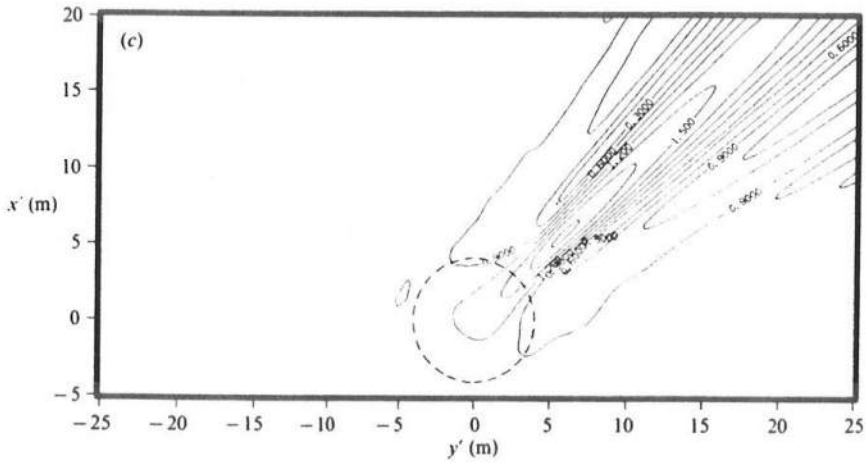

Figure 5: Envelope of the Wave Amplitude Behind a Circular Shoal for 45° of Incidence, from Dalrymple *et al.*, 1989

denote the real-valued argument of F on the line $-b \leq y \leq b$. The Fourier transform pair for f is then defined by the transform pair, (10, 11),

$$f(y) = \sum_{n=-\infty}^{\infty} \hat{f}_n \mathrm{e}^{in\lambda y}; \quad \lambda = \frac{\pi}{b} \tag{63}$$

$$\hat{f}_n = \frac{1}{2b} \int_{-b}^{b} f(y) e^{-in\lambda y} dy \tag{64}$$

Likewise, the discrete transforms ϕ_n, ν_n^2 of the physical variables $\tilde{\phi}, \nu^2$ are defined by

$$\begin{pmatrix} \tilde{\phi}(y) \\ \nu^2(y) \end{pmatrix} = \sum_{n=-\infty}^{\infty} \begin{pmatrix} \phi_n \\ \nu_n^2 \end{pmatrix} \mathrm{e}^{in\lambda y}; \quad \lambda = \frac{\pi}{b} \tag{65}$$

$$\begin{pmatrix} \phi_n \\ \nu_n^2 \end{pmatrix} = \frac{1}{2b} \int_{-b}^{b} \begin{pmatrix} \tilde{\phi}(y) \\ \nu^2(y) \end{pmatrix} \mathrm{e}^{-in\lambda y} dy \tag{66}$$

The discrete Fourier transform of the governing equation (58) gives

$$\frac{d^2\phi_n}{dx^2} + (\overline{k^2} - (n\lambda)^2)\phi_n - \overline{k^2}\hat{f}_n = 0 \tag{67}$$

By direct substitution, we obtain

$$f(y) = \sum_{l} \sum_{m} \nu_l^2 \ \phi_m \ e^{i(l+m)\lambda y} \tag{68}$$

Then

$$\begin{aligned} \hat{f}_n &= \frac{1}{2b}\int_{-b}^{b} \sum_l \sum_m \nu_l^2 \, \phi_m \, e^{i(l+m-n)\lambda y} dy \\ &= \sum_l \sum_m \nu_l^2 \, \phi_m \, \delta(l+m-n) \end{aligned} \tag{69}$$

where $\delta(s) = 1$ for $s = 0$ and zero otherwise. We thus require the condition $l + m - n = 0$ in order to obtain a contribution to the surface wave mode by the bottom. For an arbitrary choice of l and a subsequently fixed value of $m = n - l$, we obtain the expression

$$\hat{f}_n = \sum_{l=-\infty}^{\infty} \nu_l^2 \, \phi_{n-l} \tag{70}$$

When this term is substituted back into (67), it is clear that the effect of F_n is to scatter energy into (or out of) mode n through resonant interaction between a surface wave at mode $n - l$ and a bottom mode l. The interaction is a linear process, since the amplitudes ν_l^2 are fixed. The formulation may be interpreted as a generalization of the Bragg scattering mechanism described by Mei[35] for forward propagation over a sinusoidal bed (actually not explicitly covered here) and by Naciri and Mei[37] for waves propagating over a bi-periodic bottom. In this extension, the entire problem of wave deformation by a non-uniform bottom may be viewed as the result of a complicated multiple scattering problem involving the entire set of Fourier modes resolved by the system.

In practice, it is possible either to use the FFT and inverse FFT algorithms to evaluate the last term in (67), or to evaluate the sum in (70) after evaluating the FFT of ν^2. The operation count of the second option is smaller, although all exponentials involved in the computation of the FFT's may be evaluated once and then stored, making the subsequent FFT calls quite efficient.

Dalrymple and Suh[14] show this interaction between the bottom and surface modes, using an idealized bathymetry consisting of sinusoidal corrugations perpendicular to the x axis, so that the major component of the bottom was ν_2^2. The surface wave train was incident at an angle corresponding to ϕ_4 at x=0. According to (70), the next modes to be forced by the bottom are ϕ_2 and ϕ_6. These modes then create additional modes. These results are shown on Figures 6 – 8, which show the evolution of the angular spectrum with distance, x, and the instantaneous water surface. Note that wave rays, obtained from refraction theory and depicted with solid lines, are also shown.

4.4 Nonlinear Effects

The solutions discussed so far have been for linear theory, which permits the summation over many wave directions. The water wave problem however is nonlinear, due to the free surface boundary conditions. There have been two approaches to solving a more nonlinear problem. The first is to replace the linear dispersion relationship (17) used to find the wave

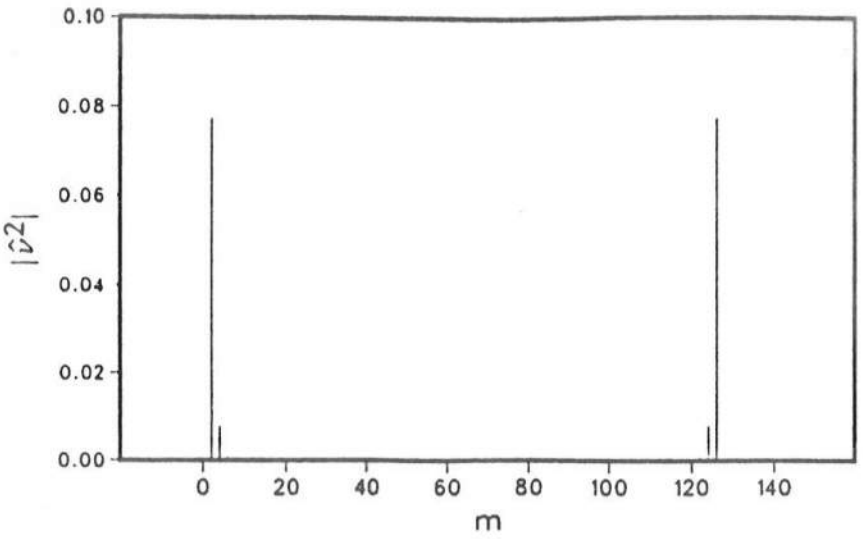

Figure 6: Amplitude Spectrum of the Bottom Modes, $\nu^2(x, m\lambda)$, from Dalrymple and Suh, 1988

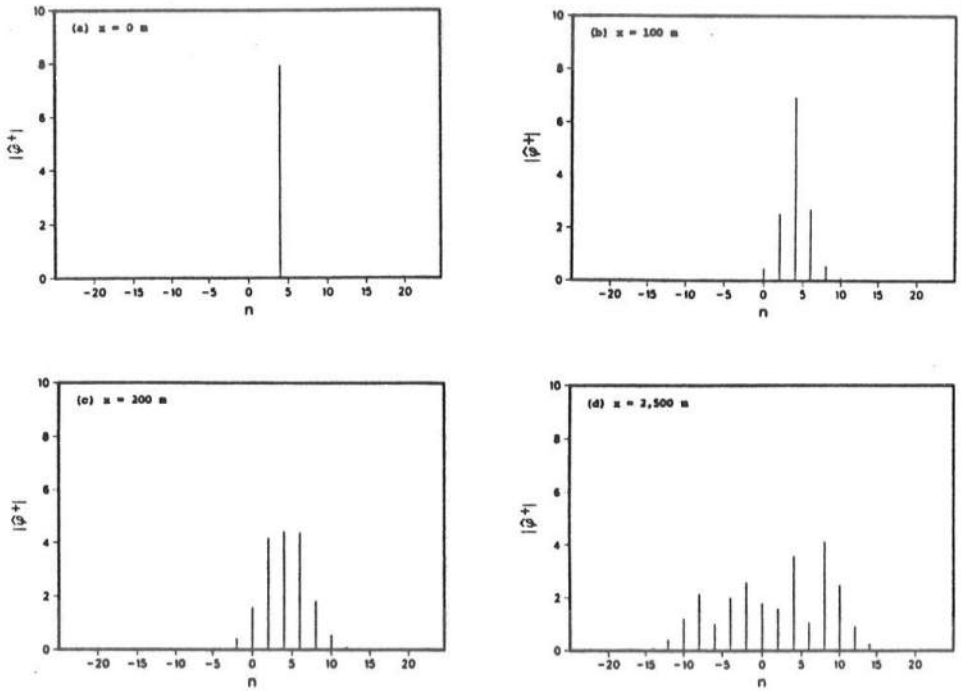

Figure 7: Evolution of the Angular Spectrum at Different x Locations, from Dalrymple and Suh, 1988

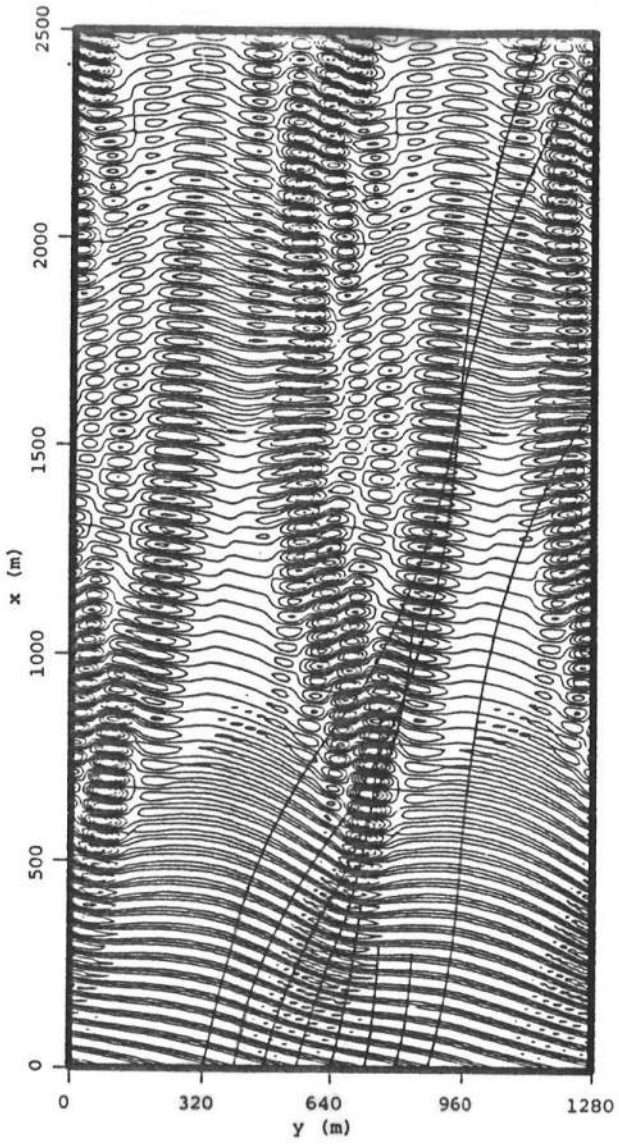

Figure 8: Instantaneous Water Surface Elevations Over Periodic Ridges, from Dalrymple and Suh, 1988

number given the wave frequency with a nonlinear dispersion relationship, which includes amplitude dispersion. Candidates for this dispersion relationship could be the Stokes third order relationship or the modified dispersion relationship of Kirby and Dalrymple.[29] This last relationship was used directly in the equations in Section 3.2, with very good agreement with laboratory data by Dalrymple *et al.*[15]

The second approach is to rigorously satisfy the nonlinear governing equations, which are

$$\nabla^2\Phi = 0 \quad (-h < z < \eta) \tag{71}$$

$$g\Phi_z + \Phi_{tt} + (|\nabla\Phi|^2)_t + \frac{1}{2}(\nabla\Phi\cdot\nabla)|\nabla\Phi|^2 = 0 \quad (z=\eta) \tag{72}$$

$$\Phi_t + \frac{1}{2}|\nabla\Phi|^2 + g\eta = 0 \quad (z=\eta) \tag{73}$$

$$\Phi_z = -\nabla_h\Phi\cdot\nabla_h h \quad (z=-h) \tag{74}$$

where ∇ and ∇_h are the three-dimensional and the horizontal gradient operators.

The methodology is to expand Φ and η in terms of a small parameter, ϵ, which is the Stokes steepness parameter,

$$\Phi = \sum_{n=1}^{\infty}\epsilon^n\phi_n; \qquad \eta = \sum_{n=1}^{\infty}\epsilon^n\eta_n \tag{75}$$

Also the method of multiple scales is used, which has been shown to be very useful for wave evolution problems.[7] Suh *et al.*[49] chose the following slow variables

$$x_1 = \epsilon x, x_2 = \epsilon^2 x, ...; t_1 = \epsilon t, t_2 = \epsilon^2 t, ... \tag{76}$$

A mild slope bottom was assumed, such that $h_x \sim \epsilon^2 h_{x_2}$. This leaves the bottom effectively characterized by straight and parallel contours up until third order. Next, the Taylor series is used to expand the nonlinear free surface boundary conditions about $z = 0$ and the bottom boundary condition about $z = -\bar{h}$, which provides for series representations of these nonlinear conditions in linear form, ordered by the Stokes parameter. Finally, grouping the coefficients of each order of the Stokes parameter gives a boundary value problem for each order, n:

$$\nabla^2\phi_n = F_n \quad (-\bar{h} < z < 0) \tag{77}$$

$$g\phi_{n_z} + \phi_{n_{tt}} = G_n \quad (z=0) \tag{78}$$

$$\phi_{n_t} + g\,\eta_n = H_n \quad (z=0) \tag{79}$$

$$\phi_{n_z} = B_n \quad (z=-\bar{h}) \tag{80}$$

where the forcing terms, F_n, G_n, H_n, B_n, are determined from solutions of lower order. See Suh *et al.*[49] for the complete expressions for the right hand sides. The first order solution, as expected, is that of Dalrymple and Kirby,[12] for waves on straight and parallel contours. At the second order, the interaction of components of the first order directional spectrum leads

to the appearance of sum and difference frequencies, including the usual Stokes harmonic. Additionally, forcing from the bottom occurs through the coupling term in Dalrymple *et al.*[15] At the third order, the forcing of the wave field is due to third-order terms proportional to the first harmonics and a cubic resonance which results from the interaction of the primary waves and the second-order sum and difference waves or among three primary waves. New bottom coupling terms arise as well.

Suh *et al.*[49] compared the third-order model to data,[2,24] showing good agreement, far better than that obtained by linear theory. Another comparison was made to the nonlinear model of Dalrymple *et al.*[15] on the BBR[2] data set, also showing good agreement and indicating that, at least for the example shown, the two methods of including nonlinearity are almost equivalent. In fact, the Dalrymple *et al.*[15] model has a computational advantage for most applications; however it does not include the wave-wave interactions as does Suh *et al.*[49] Both models have the disadvantage that for very large angles, say greater than 50° , the model results begin to show discrepancies.

5 Shallow Water Waves

As waves propagate towards shore, they enter a region where the wavelength becomes long relative to the water depth, and the product kh in the dispersion relation (17) becomes small. In this case, the dispersion relation approaches the limiting form

$$\omega^2 = gk^2h \tag{81}$$

and wave speed $C = \omega/k$ becomes only weakly dependent on frequency. In this limit, all waves are travelling at nearly the same speed, and strong nonlinear coupling exists between waves of different frequency and direction. Numerous studies have indicated that the Boussinesq equations (in which all frequencies are treated together) provide an adequate model for the wave field, prior to the onset of wave breaking. To date, this problem has only been treated (from the angular spectrum point of view) for the case of topography varying in one direction; the case of two-dimensional topography has not been described as of yet. Kirby[27] has developed a model for waves on an infinitely long beach and has compared model results to data and parabolic model results. This model will be presented here.

We first establish the form of a model for waves in a laterally unrestricted domain. Again, a Cartesian coordinate system is adopted which has x pointed in the onshore direction and y pointing alongshore. Depth is assumed to vary as $h(x)$ only. We take as a starting point the variable depth Boussinesq equations as given by Peregrine:[41]

$$\eta_t + \nabla \cdot (h\mathbf{u}) + \epsilon \nabla \cdot (\eta \mathbf{u}) = 0 \tag{82}$$

$$\mathbf{u}_t + \epsilon \mathbf{u} \cdot \nabla \mathbf{u} + g\nabla\eta = \mu^2 \{ \frac{h}{2} \nabla(\nabla \cdot (h\mathbf{u}_t)) - \frac{h^2}{6} \nabla(\nabla \cdot \mathbf{u}_t) \} \tag{83}$$

Here, η is the surface displacement and $\mathbf{u}$ is the horizontal wave-induced velocity vector. The equations are kept in dimensional form; the scaling parameters ϵ for nonlinearity and μ^2 for

weak dispersion are present only schematically and will be subsequently dropped. We will assume that either bottom slope or the amplitude of bottom features (as scaled by water depth) are also small and hence the model will be developed to leading order in nonlinearity, dispersion, and domain inhomogeneity. This leads to immediate neglect of bottom slope effects in the dispersive terms of (83). Using the linear portion of (82), we may then write (83) in the reduced form

$$\mathbf{u}_t + \mathbf{u} \cdot \nabla \mathbf{u} + g \nabla \eta + \frac{h}{3} \nabla \eta_{tt} = 0. \tag{84}$$

We now make the following two assumptions. First, the model will be applied to time-periodic wave trains, where periodicity is in the sense of either a regular wave train, or of a discrete FFT over a finite length of sampled data. This assumption has been routinely applied in the spectral sense in the one-directional shoaling model of Freilich and Guza[19] (see also Elgar and Guza[18]). Its interpretation in the regular wave case is straightforward, with the wave being separated into its harmonic components (Rogers and Mei;[44] Liu, Yoon and Kirby,[32] hereafter referred to as LYK). Secondly, the wave field will be assumed to be periodic in the transverse y direction. This corresponds again to a fixed longshore wavelength in the regular wave case, or to periodicity over a long spatial interval in the spectral sense.

The governing equations are first split into coupled elliptic models for separate harmonic components. Following LYK, the surface displacement and velocity are written as

$$\eta = \sum_{n=0}^{N} \frac{\eta_n(x,y)}{2} \mathrm{e}^{-in\omega t} + c.c. \tag{85}$$

$$\mathbf{u} = \sum_{n=0}^{N} \frac{\mathbf{u}_n(x,y)}{2} \mathrm{e}^{-in\omega t} + c.c. \tag{86}$$

Substitution of (85) and (86) in (82) and (84) and subsequent elimination of the velocity leads to the following model equation for the η_n in the horizontal plane:

$$n^2\omega^2 \eta_n + \nabla \cdot (G_n \nabla \eta_n) + [n.l.t.]_n = 0; \qquad n = 1, ..., N \tag{87}$$

Here, $[n.l.t]_n$ denotes the nonlinear interactions with other discrete frequency components which are sorted by means of the rules for triad interactions applied to the time dependence; complete expressions may be found in Kirby.[27] The mode $n = 0$ corresponding to the steady, wave-induced setdown is neglected since it is at most second order in the largest wave amplitudes present (see LYK). Also,

$$G_n(x) = gh(x) - \frac{1}{3} n^2 \omega^2 h^2(x). \tag{88}$$

We now Fourier transform the wave field in the y direction, assuming propagation is to be considered in the on-offshore ($\pm x$) direction. We consider here the case of an unbounded lateral domain and a wave field which is periodic over the basic interval $-b < y < b$. We then represent $\eta_n(x,y)$ as

$$\eta_n(x,y) = \sum_{m=-M}^{M} \eta_n^m(x) \mathrm{e}^{im\lambda y} \tag{89}$$

where

$$\lambda = \frac{\pi}{b}. \tag{90}$$

as before. Substituting (89) in (87) and neglecting x - derivatives of small terms in G_n then leads to a set of coupled second-order ODE's for the η_n^m, given by

$$\frac{G_n}{gh}\eta^m_{n,xx} + \frac{h_x}{h}\eta^m_{n,x} + (\gamma_n^m)^2\eta_n^m + \frac{1}{3}m^2n^2\lambda^2k^2h^2\eta_n^m + \frac{1}{gh}[n.l.t.]_n^m = 0;$$
$$n = 1, ..., N; \qquad m = -M, ..., M. \tag{91}$$

where $[n.l.t.]_n^m$ now represents triad interactions satisfying resonance conditions in t and y. Here, k is the wavenumber determined by the lowest order dispersion relation (81). Also,

$$(\gamma_n^m)^2 = n^2k^2 - m^2\lambda^2 \tag{92}$$

For fixed n, k, λ, large values of m will make γ_n^m imaginary, which corresponds to modes which are exponential rather than oscillatory in x in the linear approximation. In the linear case, the presence of these modes in the boundary conditions would be interpreted in the same light as the presence of evanescent modes in the wavemaker problem discussed in Section 2.1.1. However, the interpretation in the case of possible nonlinear forcing of the offshore portion of trapped modes in the nearshore region is non-trivial and will need to be considered carefully in applications where the inclusion of this effect is desired. In addition, nonlinearity could force the propagation of modes that would not be present in a linearized wave field, and which could affect a detailed representation of an individual wave. At present, the range of M at each value of n may be restricted to $M_n \leq nk/\lambda$ in order to eliminate forcing of these modes arbitrarily.

5.1 Shoaling waves

The model developed in the previous section allows for the onshore and offshore propagation of the directional spectrum components. Here, attention is restricted to waves propagating onshore, or in the positive sense with respect to the x coordinate.

Based on the linear, nondispersive portion of the model (91), we assume that the incident wave may be written in the form

$$\eta_n^m(x) = A_n^m(x)\mathrm{e}^{in\int k\tilde{\gamma}_n^m \mathrm{dx}} \tag{93}$$

where it is assumed that the x dependence of A, k and $\tilde{\gamma}$ is on a slow scale of $O(\epsilon)$, and where

$$\tilde{\gamma}_n^m = (1 - (\frac{m}{n})^2(\frac{\lambda}{k})^2)^{1/2} = \frac{\gamma_n^m}{nk} \tag{94}$$

(where the positive root is taken). The amplitudes A represent the discrete angular spectrum being considered here, and are allowed to vary owing to refraction, shoaling, dispersion and nonlinear interaction. (It would be possible to absorb shoaling and refraction effects by the

use of the usual linear refraction formulae; this step is not taken here.) Substitution of (93) in (91) leads to the spectral model for incident waves, given by

$$\tilde{\gamma}_n^m A_{n,x}^m + \frac{(kh\tilde{\gamma}_n^m)_x}{2kh} A_n^m - \frac{1}{6} in^3 k^3 h^2 A_n^m$$
$$+\frac{ink}{8h}\left\{\sum_{l=1}^{n-1}\sum_{p=P_1}^{P_2} I_{n,l}^{m,p} A_l^p A_{n-l}^{m-p} e^{i\int \Theta_{n,l}^{m,p} dx} + 2\sum_{l=1}^{N-n}\sum_{p=P_3}^{P_4} J_{n,l}^{m,p} A_l^{p*} A_{n+l}^{m+p} e^{i\int \Upsilon_{n,l}^{m,p} dx}\right\} = 0;$$
$$n = 1, ..., N; \qquad m = -M_n, ..., M_n. \tag{95}$$

Here, $(\cdot)^*$ denotes the complex conjugate. The limits of summation $P_1 - P_4$ are given by

$$\begin{aligned} P_1 &= \max(-M_l, -M_{n-l} + m) \\ P_2 &= \min(M_l, M_{n-l} + m) \\ P_3 &= \max(-M_l, -M_{n+l} - m) \\ P_4 &= \min(M_l, M_{n+l} - m) \end{aligned} \tag{96}$$

The interaction coefficients I and J are given by

$$I_{n,l}^{m,p} = 1 + [\tilde{\gamma}_l^p \tilde{\gamma}_{n-l}^{m-p} + \frac{p}{l}\frac{m-p}{n-l}(\frac{\lambda}{k})^2] \cdot [1 + (\frac{m}{n})^2(\frac{\lambda}{k})^2 + \frac{(l\tilde{\gamma}_l^p + (n-l)\tilde{\gamma}_{n-l}^{m-p})^2}{n^2}] \tag{97}$$

$$J_{n,l}^{m,p} = I_{n,-l}^{m,-p}. \tag{98}$$

The phase arguments Θ and Υ represent the basic mismatch in the x direction of the triads chosen based on perfect matching in y and t. Generally, the only components which experience complete resonance in the long wave limit must have parallel propagation directions; all obliquely interacting components are somewhat detuned. The phase arguments are given by

$$\Theta_{n,l}^{m,p} = lk\tilde{\gamma}_l^p + (n-l)k\tilde{\gamma}_{n-l}^{m-p} - nk\tilde{\gamma}_n^m \tag{99}$$

$$\Upsilon_{n,l}^{m,p} = \Theta_{n,-l}^{m,-p} \tag{100}$$

The spectral model (95) is a set of coupled first order ODE's which are solvable by standard techniques. Results were obtained using a 4th-order Runge-Kutta scheme.

5.2 Comparison with Laboratory Data

In order to verify the basic computational model provided by (95), Kirby[27] compared model predictions to the laboratory data obtained by Hammack *et al.*[22] for the case of glancing, or Mach, reflection of a cnoidal wave by a vertical wall. Additional comparisons were made with parabolic models. The experimental tests were conducted using the directional wave maker at the Coastal Engineering Research Center, Vicksburg, MS. A prior use of this facility to study the properties of intersecting cnoidal waves is described in Hammack *et al.*,[21] referred to here as HSS, who also discuss the instrumentation and data acquisition used.

For the tests considered here, the wave basin was operated with a water depth of $20cm$ in a constant depth region extending $12.55m$ in front of the wavemaker, after which a beach with 1:30 slope provided an efficient wave absorber giving little reflection. For the Mach stem tests, two parallel false walls were installed perpendicular to the wavemaker axis in order to provide a closed channel. The channel walls were situated $13.26m$ apart, which fixes the width of the numerical domain to be considered.

The generation of oblique cnoidal waves using the directional wavemaker has been described in HSS. In the present laboratory tests, waves were initially specified as having a wavelength of $2m$ and a crest elevation $4cm$ above mean water level.

A sample of the model calculations is presented here as gray level contour plots of instantaneous surface over the model basin. The gray level plots are actually of the quantity $-\partial\eta/\partial x$, and the pictures thus mimic the visual image that would be obtained in an overhead photograph resulting from lighting at a low angle from the direction of the wavemaker. (This is similar to the photographic arrangement in HSS). Figure 9 presents results for the test CR150204, which clearly shows the evolution of a wide Mach stem wave along the reflecting boundary. In contrast, Figure 10 shows the other extreme example of test CR580204, where the angle of incidence is about 45° and the reflection pattern is regular (i.e., nearly linear superposition.) The reader is referred to Kirby[27] for a detailed comparison between model results and the laboratory data.

A summary of the results of that comparison is indicated in Figure 11, where an rms error estimate, based on differences between measured and computed wave profiles at 9 gage locations, is presented. The error is shown as a function of incident wave angle, and results are given for the present angular spectrum model (solid line) and the parabolic equation method model described in Liu, Yoon and Kirby[32] (dashed line). The results indicate that the present model provides a better estimate of the measured wave field at all angles of incidence. The results also indicate that the accuracy of the prediction decreases with increasing angle of incidence for both models. This would not be expected for the present angular spectrum model, which should provide accurate predictions at large angles of incidence. Part of the discrepancy is due to an error in the original experimental wave generation that led to the generated waves being initially higher than desired, with the error increasing with increasing angle of incidence. This error and its interaction with the numerical predictions will be discussed in more detail in a subsequent publication, and direct comparisons between numerical results of the present model and results of a solution of the full Boussinesq equations will be described.

6 Conclusions

The angular spectrum method for both intermediate and shallow water depths provides a useful tool for the propagation of water waves. It has the advantage of including refraction, diffraction, and shoaling, but permitting larger angles of propagation than the parabolic models permit.

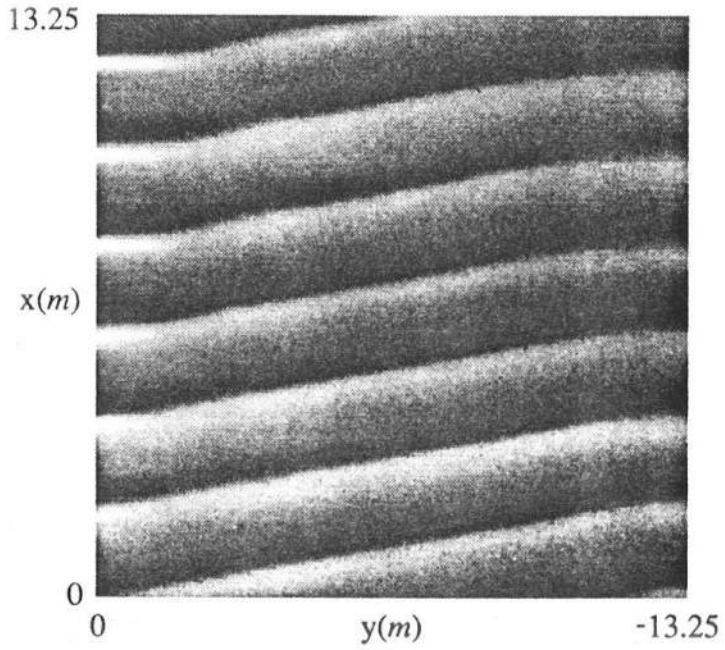

Figure 9: Reflection of Cnoidal Wave from Barrier, Corresponding to TEST CR150204 (Kirby, 1990)

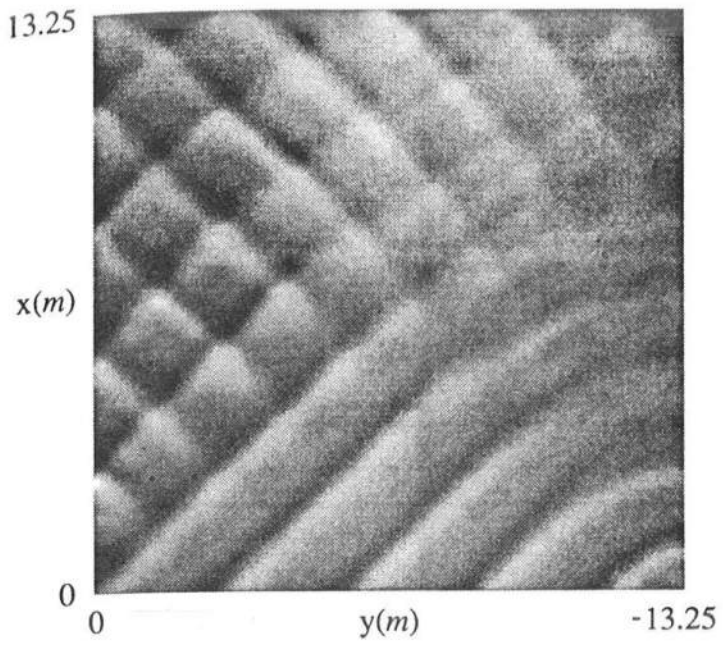

Figure 10: Reflection of Cnoidal Wave from Barrier, Corresponding to TEST CR580204 (Kirby, 1990)

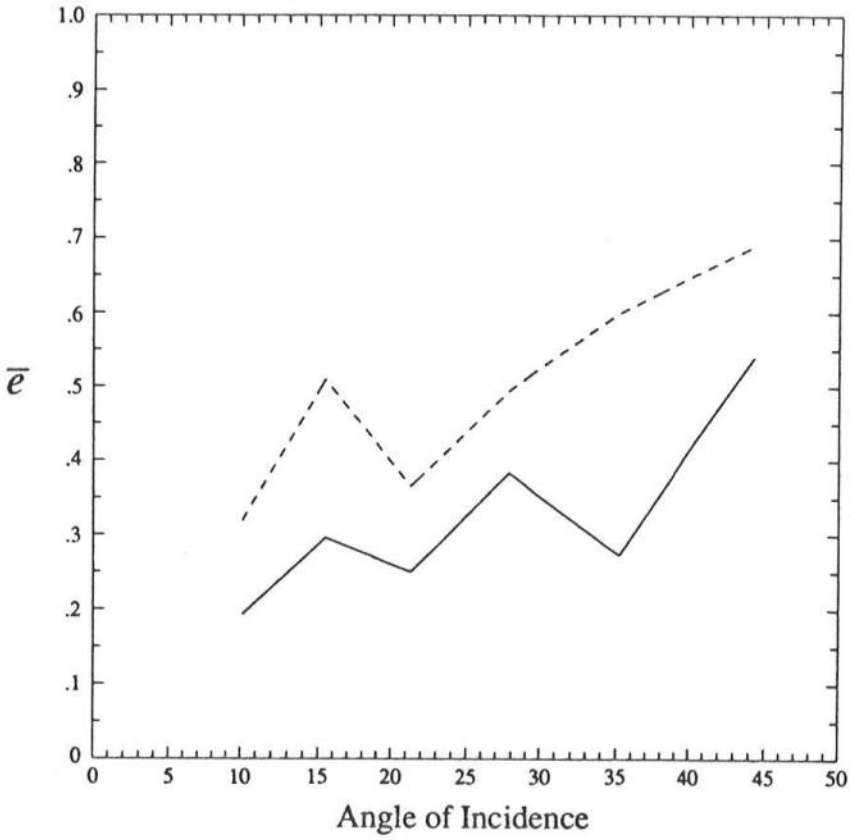

Figure 11: Variation of rms error measure with angle of incidence θ. Solid line - angular spectrum model, Dashed line - parabolic model.

The angular spectrum provides an interesting interpretation of diffraction. For the case of diffraction through a gap, treated by the Kirchoff approximation, the initial condition contains all the information for diffraction. The circular spreading of waves behind a gap is simply the radial spreading associated with the different propagation directions of the Fourier modes. There is no coupling between the modes when there is no lateral variation in bathymetry. Further for cases where diffraction occurs within the computational domain, say, behind a shoal surrounded by constant depth water, the coupling between the bottom modes and the surface wave modes over the shoal forces new modes to grow which, behind the shoal, lead to the characteristic focus and diffraction regions. However, for linear wave models, there is no coupling between the modes after the waves pass over the (refractive) shoal region.

In shallow water, the mode coupling is very strong and plays a major role in the computations. However, comparisons to data show that the angular spectrum model is very good; in fact, better than parabolic representations of the Boussinesq equations.

Future work in angular spectrum modelling will be directed to the development of an elliptic angular spectrum model to provide for reflection upwave and the application to a full directional spectrum by superposing many frequencies.

Acknowledgments

Much of RAD's efforts in angular spectrum modelling have been supported by the Dept. of Commerce's Sea Grant Program through grants to the University of Delaware. JTK's work was supported by the Office of Naval Research through contracts N00014-86-K-0790, N00014-89-J-1717, and N00014-90-J-1678. Both would like to acknowledge Dr. K.D. Suh, who participated in the development of the irregular bathymetry and nonlinear versions of the angular spectrum model.

7 References

References

[1] Berkhoff, J.C.W., Computation of combined refraction-diffraction, *Proc. 13 th Intl. Conf. Coastal Engrg.,* ASCE, 471-490, 1972.

[2] Berkhoff, J.C.W., N. Booij, and A.C. Radder, Verification of numerical models for simple harmonic linear waves, *Coastal Engineering*, 6, 255-279, 1982.

[3] Bettess, P. and O.C. Zienkiewicz, Diffraction and refraction of surface waves using finite and infinite elements, *Int. J. Numerical Meth. in Eng.*, 11, 1271-129, 1977.

[4] Booij, N., Gravity waves on water with non-uniform depth and current, Department of Civil Engrg., Tech. Univ. Delft, Rpt. 81-1, 1981.

[5] Booker, H.G. and P.C. Clemmow, The concept of an angular spectrum of plane waves, and its relation to that of polar diagram and aperture distribution, *Proc. Instn. Elect. Eng.*, Pt III, 97, 11, 1950.

[6] Born, M. and Wolf, E., *Principles of Optics*, 5^{th} Ed., Pergamon Press, New York, 808pp., 1975.

[7] Chu, V.H. and Mei, C.C., On slowly-varying Stokes waves, *Journal Fluid Mech.*, 41, 873-887, 1970.

[8] Clemmow, P.C., **The Plane Wave Spectrum Representation of Electromagnetic Fields,**, Pergamon Press, Oxford, 185pp, 1966.

[9] Dalrymple, R.A., A model for the refraction of water waves, *J. Waterway, Port, Coastal and Ocean Engrg.*, ASCE, 114, 4, 423-435, 1988.

[10] Dalrymple, R.A., Directional wavemaker theory with sidewall reflection, *J. Hyd. Res.*, 27, 1, 1989.

[11] Dalrymple, R.A. and M. Greenberg, Directional wavemakers, in **Physical Modelling in Coastal Engineering,** R.A. Dalrymple, ed., A.A. Balkema, Rotterdam, 1985.

[12] Dalrymple, R.A. and J.T. Kirby, Models for very wide angle water waves and wave diffraction, *J. Fluid Mech.*, 192, 33-50, 1988.

[13] Dalrymple, R.A. and P.A. Martin, Wave diffraction through offshore breakwaters, *J. Waterway, Port, Coastal and Ocean Engrg.*, 116, 6, ASCE, 1990.

[14] Dalrymple, R.A. and K. Suh, Wide–angle water wave models using Fourier method, *Proc.* 21^{st} *Int. Conf. Coastal Engrg.*, ASCE, Torremolinos, 246-260, 1988.

[15] Dalrymple, R.A., K. Suh, J.T. Kirby and J.W. Chae, Models for very wide angle water waves and wave diffraction, part 2. Irregular bathymetry *J. Fluid Mech.*, 201, 299-322, 1989.

[16] Dean, R.G. and Dalrymple, R.A., **Water Wave Mechanics for Engineers and Scientists**, Prentice-Hall, Englewood Cliffs, 353 pp., 1984; reprinted by World Scientific, Singapore, 1990.

[17] Ebersole, B.A, Refraction-diffraction model for linear water waves, *J. Waterway, Port, Coastal and Ocean Engrg.h*, 111, 6, ASCE, 1985.

[18] Elgar, S. and R.T. Guza, Shoaling gravity waves: comparisons between field observations, linear theory, and a nonlinear model, *J. Fluid Mech.*, 158, 47-70, 1985.

[19] Freilich, M.H. and R.T. Guza, Nonlinear effects on shoaling surface gravity waves, *Phil. Trans. Roy. Soc. Lond.*, A, 31, 1-41, 1984.

[20] Goodman, J.W., **Introduction to Fourier Optics**, San Francisco: McGraw-Hill, pp 287, 1968.

[21] Hammack, J., N. Scheffner and H. Segur, Two-dimensional periodic waves in shallow water, *J. Fluid Mech.*, 209, 567-589, 1989.

[22] Hammack, J., N. Scheffner and H. Segur, personal communication, 1990.

[23] Houston, J.R., Combined refraction and diffraction of short waves using the finite element method, *Applied Ocean Research*, 3, 163-170, 1981.

[24] Ito, Y. and K. Tanimoto, A method of numerical analysis of wave propagtioan: application to wave diffraction and refraction, *Proc. 13 th Intl. Conf. Coastal Engrg.*, ASCE, Vancouver, 503-522, 1972.

[25] Kirby, J.T., Higher-order approximations in the parabolic equation method for water waves, *J. Geophys. Res.*, 91, 933-952, 1986a.

[26] Kirby, J. T., Rational approximations in the parabolic equation method for water waves, *Coastal Engineering*, 10, 355-378, 1986b.

[27] Kirby, J.T., Modelling shoaling directional wave spectra in shallow water, *Proc. 22nd Intl. Conf. Coastal Engrg.*, ASCE, Delft, 1990.

[28] Kirby, J.T. and R.A. Dalrymple, A parabolic equation for the combined refraction-diffraction of Stokes waves by mildly varying topography, *J. Fluid Mech.*, 136, 453-466, 1983.

[29] Kirby, J.T. and R.A. Dalrymple, An approximate model for nonlinear dispersion in monochromatic wave propagation models, *Coastal Engineering*, 9, 1986.

[30] Liu, P.L.-F. and C.C. Mei, Water motion on a beach in the presence of a breakwater, I. Waves *J. Geophys. Res.*, 81, 18, 3079-3084, 1976.

[31] Liu, P.L.-F. and T.K. Tsay, Refraction-diffraction model for weakly nonlinear water waves, *J. Fluid Mech.*, 141, 265-274, 1984.

[32] Liu, P.L-F., Yoon, S.B. and Kirby, J.T., 1985, Nonlinear refraction-diffraction of waves in shallow water, *J. Fluid Mech.*, 153, 185-201.

[33] Lozano, C.J. and P.L.-F. Liu, Refraction-diffraction model for linear surface water waves, *J. Fluid Mech.*, 101, 1980.

[34] Mei, C. C., Resonant reflection of surface water waves by periodic sandbars, *J. Fluid Mech.*, 152, 315-335, 1985.

[35] Mei, C.C., Tlapa, G.A. and P.S. Eagleson, An anymptotic theory for water waves on beaches of mild slope, *J. Geophys. Res.*, 73, 4555-4560, 1968.

[36] Munk, W.H. and R.S. Arthur, Wave intensity along a refracted ray in gravity waves, Natl. Bur. Stand. Circ. 521, Washington, D.C., 1952.

[37] Naciri, M. and Mei, C. C., Bragg scattering of water waves by a doubly periodic seabed, *J. Fluid Mech.*, 192, 51-74, 1988.

[38] Noda, E.K., Wave-induced nearshore circulation, *J. Geophys. Res.*, 79, 27, 4097-4106, 1974.

[39] Papoulis, A., **The Fourier Integral and Its Applications**, McGraw Hill Book Company, New York, 1662.

[40] Penney, W.G. and A.T. Price, The diffraction theory of sea waves and the whelter afforded by breakwaters, *Philos. Trans. Roy. Soc.*, A, 244(882), 236-253, 1950.

[41] Peregrine, D.H., Long waves on a beach, *J. Fluid Mech.*, 27, 815-827, 1967.

[42] Perlin, M. and R.G. Dean, An efficient numerical agorithm for wave refraction/shoaling problems, *Proc. Coastal Structures, 83*, ASCE, 988-999, 1983.

[43] Radder, A.C, "On the parabolic equation method for water-wave propagation", *J. Fluid Mech.*, 95, 1, 159-176, 1979.

[44] Rogers, S.R. and C.C. Mei, Nonlinear resonant excitation of a long and narrow bay, *J. Fluid Mech.*, 88, 161-180, 1978.

[45] Sommerfeld, A., Mathematische Theorie der Diffraction, *Math. Ann.*, 47, 317-374, 1898.

[46] Smith, R. and Sprinks, T., Scattering of surface waves by a conical island, *J. Fluid Mech.*, 72, 2, 373-384, 1975.

[47] Stamnes, J.J., **Waves in Focal Regions : Propagation, Diffraction and Focussing of Light, Sound and Water Waves**, Adam Hilger, Boston, 1986.

[48] Stamnes, J.J., Lovhaugen, O., Spjelkavik, B., Mei, C.C., Lo, E. and Yue, D.K.P., Nonlinear focussing of surface waves by a lens–theory and experiment, *J. Fluid Mech.*, 135, 71-94, 1983.

[49] Suh, K.D., R.A. Dalrymple, and J.T. Kirby, An angular spectrum model for propagation of Stokes waves, *J. Fluid Mech.*, 221, 205-232, 1990.